Local Structure and Orientational Ordering in Liquid Bromoform

Jacob J. Shephard,[a] John S. O. Evans[b] and Christoph G. Salzmann[c]*

[a] *Department of Chemistry, University of Edinburgh, David Brewster Road, Edinburgh EH9 3FJ, UK;* [b] *Department of Chemistry, Durham University, South Road, Durham DH1 3LE, UK;* [c] *Department of Chemistry, University College London, 20 Gordon Street, London WC1H 0AJ, UK*

* c.salzmann@ucl.ac.uk

Local Structure and Orientational Ordering in Liquid Bromoform

The neutron diffraction data of liquid bromoform ($CHBr_3$) at 25°C was analysed using the Empirical Potential Structure Refinement technique in combination with H/D isotopic substitution. Compared to liquid chloroform ($CHCl_3$), $CHBr_3$ displays more spatially defined intermolecular contacts. A preference for polar stacking with collinear alignment of dipole moments is observed for the most closely approaching $CHBr_3$ molecules, although to a lesser extent than in chloroform. Consistent with this and in line with dielectric spectroscopy, the Kirkwood correlation factor from the structural model of $CHBr_3$ is smaller than that of $CHCl_3$. The net antiparallel alignment of dipole moments in $CHBr_3$, as suggested by dielectric spectroscopy, must be due to weak but persistent long-range orientation correlations in $CHBr_3$, which counteract the local polar stacking.

Keywords: bromoform; haloforms; neutron diffraction; Kirkwood correlation factor

Introduction

Trihalomethanes (CHX_3) are important in a wide range of environmental settings and industrial applications.[1] To emphasise the chemical similarities with formic acid, they are often called haloforms and can be prepared using the well-known haloform reaction.[2] Fluoroform (CHF_3) is a non-ozone depleting greenhouse gas that is used in refrigeration.[3] Both chloroform ($CHCl_3$) and bromoform ($CHBr_3$) are solvents with high densities and are often used for extraction processes. Famous examples include the extraction of morphine from poppies[4] and atropine from thorn apple leaves.[5] Iodoform (CHI_3) is solid at room temperature and used as a disinfectant whose distinctive smell is often associated with hospitals. The crystal structure of CHI_3 displays disorder with respect to the either parallel or antiparallel alignments of the molecular dipole moments in line with the nonpolar 6/*m* point-group symmetry of $P6_3/m$.[6] Similar types of disorder are also observed for the high-temperature / low-pressure phases of $CHBr_3$ and $CHCl_3$.[7]

Recently, the local structure of liquid $CHCl_3$ was investigated by analysing X-ray and neutron diffraction data of H/D isotopically substituted samples[8] with the Empirical Potential Structure Refinement (EPSR) technique.[9] This study suggested a very strong tendency for polar stacking of $CHCl_3$ molecules with collinear alignments of the dipole moments. In fact, the extent of orientation correlations in $CHCl_3$ was found to exceed even those previously found in liquid hydrogen chloride[10] as well as in a wide range of other polar liquids.[10,11,12] These findings are to some extent in contrast to the conclusions of two earlier diffraction studies.[13,14] The earliest work suggested that the most favourable arrangement of two molecules in liquid $CHCl_3$ is one in which the dipole axes are inclined with respect to each other.[13] However, a later study of the same data using a Reverse Monte Carlo (RMC) approach[15] for structure

reconstruction concluded that antiparallel dipole alignments dominate at low intermolecular distances.[16] More recently, an analysis of a combined neutron / X-ray diffraction dataset, also using RMC, proposed that the strongest dipole-dipole correlations are anti-collinear with the fully chlorinated faces of two molecules approaching each other.[14,17] To emphasise the validity of the EPSR structural model, Shephard *et al.* argued that a tendency for collinear alignments of the dipole moments in liquid chloroform is consistent with dielectric spectroscopy measurements.[8] A recent molecular dynamics simulation confirmed the existence of such 'super-dipoles' in relative populations that agree with experiment and the importance of local packing effects was highlighted.[18] In the chloroform acetone azeotrope, the polar aggregates were found to be disrupted to some extent by the presence of acetone.[19]

Liquid $CHBr_3$ has received much less attention so far.[1] Pothoczki *et al.* conducted a combined X-ray / neutron diffraction study and they fitted their data using RMC.[14,17] For structural analysis, an approach previously developed for CCl_4 was used,[20] which analyses the local structures in terms of the relative coordination geometries of two tetrahedra. In comparison to $CHCl_3$, it was suggested that the ratio of corner-to-face arrangements is more than twice as likely in $CHBr_3$, whereas the importance of face-to-face configurations decreases. However, based on this analysis, it is difficult to conclude on any orientation correlations of their dipole moments. The gas-phase dipole moment of $CHBr_3$ is only about 2% smaller than that of $CHCl_3$.[6]

Here we investigate the local structure of liquid $CHBr_3$ in detail by analysing neutron diffraction data of H/D isotopically substituted samples with the EPSR technique.[9] The structural characteristics of $CHBr_3$, including angle-dependent pair-correlation and orientation-correlation functions, are compared with those of

chloroform. Furthermore, the Kirkwood correlation factor from the structural model will be benchmarked against the value obtained from dielectric spectroscopy.

Materials and methods

Neutron diffraction experiment

Protiated and deuterated bromoform was purchased from Sigma Aldrich with purities of 99.9 weight% and 99.96 D / H atom%, respectively, and used without further purification.

$Ti_{0.68}Zr_{0.32}$ null-scattering alloy sample cells with internal dimensions of 1 × 38 × 38 mm were used to contain the two neat liquids as well as a 50 mol% mixture of $CHBr_3$ and $CDBr_3$ for the neutron scattering measurements. These were carried out at 25°C for ~1000 μA h of proton current on the Small Angle Neutron Diffractometer for Amorphous and Liquid Samples (SANDALS) at the ISIS spallation neutron source at the Rutherford Appleton Laboratory, UK. SANDALS detects neutrons scattered at angles between 3.9 and 39°, and covers a wavevector-transfer, Q, range of 0.1 – 50 $Å^{-1}$. The raw diffraction data were corrected for absorption and multiple scattering using the GudrunN software package, which was also used to subtract the perturbation to the data caused by inelastic collisions.[21] The inelasticity features were removed using the Iterate Gudrun routine in GudrunN to give the total structure factors, $F(Q)$, of the three liquids.

Structure reconstruction using the Empirical Potential Structure Refinement (EPSR) technique

To produce a suitable starting structure for modelling the experimental diffraction data of liquid bromoform, a standard Monte Carlo simulation was carried out using the EPSR (empirical potential structure refinement) program.[9] For this, a cubic box with

dimensions of 60.16 Å was filled with 1500 bromoform molecules giving an atomic density of 0.03444 atoms $Å^{-3}$, consistent with the experimental density at 25°C.[22] The average bond lengths and angles of bromoform were taken from a microwave experiment with small adjustments to give a better fit to the diffraction data,[23] and the Lennard-Jones parameters and partials charges from ref. [24]. The full list of parameters is summarized in Table 1. After this, the empirical potentials were switched on and the EPSR simulation was run in order to obtain the best possible fits to the data and to accumulate configurations for structural analyses.

Structural analysis of the EPSR model

The isotropic and angle-dependent pair-correlation functions as well as angle-dependent orientation-correlation functions were obtained from the EPSR model by fitting generalized spherical harmonic functions[25,26] to the partial structure factors using the EPSR auxiliary routines SHARM and SDF. The spherical harmonic functions made use of the following Clebsch-Gordon coefficients: l = 0, 1, 2, 3, 4; l_1 = 0, 1, 2, 3, 4; l_2 = 0, 1, 2, 3, 4; n_1 = 0, 1, 2, 3, 4; n_2 = 0, 1, 2, 3, 4. The various correlation functions were visualised using the plot2D or plot3D programs within the EPSR software package.

Results and discussion

Structural model of liquid bromoform

The experimental total structure factors of $CHBr_3$, $C(H/D)Br_3$ and $CDBr_3$ together with the fits to the data obtained before and after switching on the empirical potentials are shown in Figure 1(a). Allowing the empirical potentials to develop was found to improve the fit to the first strong diffraction features, which is crucial for obtaining accurate intermolecular structural information.[27] These improvements to the fits nicely illustrate the additional descriptive power of the empirical potentials compared to

a standard Monte Carlo simulation, and ensure that the structural model is consistent with the experimental data.

Figure 1(b) shows the intramolecular part of the experimental total pair-correlation function $G(r)$ of $CDBr_3$. It can be seen that the intramolecular distances used to define the molecules in the EPSR model, as indicated by the dashed lines, agree very well with the low-r peaks in $G(r)$.

In addition to the neutron diffraction experiments, we attempted to record the X-ray total structure factor of $CHBr_3$ on a lab-based silver anode X-ray diffractometer. However, most likely due to the strong absorption properties of the electron-rich $CHBr_3$, this was not possible. Nevertheless, the X-ray $F(Q)$ was calculated from our neutron-derived EPSR model, as shown in Figure 1(c), and compared with the X-ray data shown in Figure 1(d) in ref. [14]. The two $F(Q)$s agreed very well with respect to the positions, relative intensities and shapes of the various diffraction features including two weak features at 1.4 and 3.3 $Å^{-1}$.

The isotropic intermolecular pair-correlation functions, $g_{A–B}(r)$s, obtained from the EPSR model of bromoform are shown in Figure 2 together with the corresponding data of liquid chloroform from ref. [8]. Compared to chloroform, most of the peak maxima in the bromoform data are shifted towards slightly larger distances, which reflects the larger van der Waals volume of $CHBr_3$ compared to $CHCl_3$. Apart from this, the pair-correlation functions involving carbon atoms are quite similar for the two haloforms implying similar spherically-averaged structures from the perspective of the centres of the molecules. The oscillations in $g_{C–C}(r)$, with maxima at 5.6, 10.2 and 15.2 Å, indicate positional ordering reaching into at least the third coordination shell.

Inspection of the isotropic pair-correlation functions involving hydrogen and halogen atoms highlights pronounced structural differences between the two haloforms,

which are not captured from the spherically-averaged viewpoint of the carbon atoms. Significantly, a much greater probability for close H–H pairs is found in bromoform together with spatially more defined close X–X and H–X contacts.

To investigate the local structure in more detail, angle-dependent intermolecular pair-correlation functions were obtained from the EPSR model in a next step. For these analyses, the C atom of a reference molecule is positioned at the origin of the coordinate system, the H atom along the z_1 axis and one of the Br atoms in the x_1z_1-plane as shown in Figure 3(a). The position of, for example, the H atom of a 2nd molecule is then defined by a set of spherical coordinates including the radial C–H distance, r, as well as the polar and azimuthal angles θ and ϕ. The probability of the position of the H atom of a 2nd molecule with respect to the C atom of the reference molecule is reflected by the $g_{C–H}(r, \theta, \phi)$ correlation function.

The most likely positions of H atoms in the coordination shell of $CHBr_3$ can be seen from the $g_{C–H}(r, \theta)$ function shown in Figure 3(b). This function is averaged over ϕ, and therefore depends only on the radial C–H distance and θ. The majority of the most closely approaching H atoms are found at θ=180° (r=3.5 Å), and there is only a slightly increased probability at θ=±52°.

Three-dimensional structural information can be displayed using spatial density functions (SDFs), which make use of fractional isosurface levels. These highlight volumes where the pair-correlation function takes large values and contains specified fractions of the atoms.[28] The dashed circle in Figure 3(b) indicates the upper C–H distance limit of 4.7 Å used for the construction of the C–H SDF shown in Figure 3(c). Again, it can be seen that the most likely position of hydrogen atoms is in the $–z_1$ direction below the fully brominated face of the reference molecule, which suggests the

existence of polar stacks of molecules with collinear dipole alignment as has also been observed for chloroform.[8]

The most likely locations of the closest Br atoms are found at $\theta = \pm 37°$ and r=3.9 Å as well as at θ=180° and r=4.3 Å (Figure 3(d)). The three lobes in the C–Br SDF in $+z_1$ direction in Figure 3(e) show that the most likely positions of Br atoms above the reference molecule are located between the gaps of two bromine atoms of the reference molecule. Below the reference molecule, bromine atoms are most likely found below the centre of the fully brominated face. We emphasise that the structural information displayed in the SDFs in Figure 3(c,e) is consistent with the highlighted importance of corner-to-face geometries by Pothoczki *et al*.[14,17] Although, based on the three lobes in $+z_1$ direction in the SDF in Figure 3(e), it is not possible to distinguish between Br–Br–Br face to H corner, Br–Br edge to H–Br edge, H–Br edge to H–Br edge or Br corner to Br–H–Br face geometries. However, the fact that close hydrogen atoms are likely to coordinate at the Br–Br–Br face of the reference molecule (Figure 3(c)) suggests that the hydrogen atom of the reference molecule also faces a substantial fraction of Br–Br–Br faces.

Detailed information on the relative orientations of the dipole moments of neighbouring molecules can be obtained from orientation-correlation functions (OCFs).[12,25,29] Since molecules rotate about their centres of mass (COMs), the origin of the coordinate system is now placed at the COM of the reference molecule and its dipole moment is aligned with the z_1 axis. The relative orientation of the dipole moment of a 2nd molecule with respect to the dipole moment of the reference is then defined by the angle α shown in Figure 4(a). The contour plots in Figure 4(a) show the OCFs, $g_{\mathrm{COM–COM}}(r, \alpha)$, when the second molecule is located at θ angles of 0, 45, 90, 135 and 180°.

Overall, it is important to note that the orientation correlations in bromoform are less pronounced compared to those in chloroform as indicated by weaker maxima in the OCFs.[8] The positions labelled with (1), (2) and (3) in Figure 4(a) correspond to the molecular arrangements shown in Figure 4(b). Despite weaker orientation correlations, there is a tendency for stacking of molecules with collinear dipole alignment as observed for chloroform (structure 1). Neighbouring molecules with hydrogen atoms close to the Br–Br–Br face of the reference molecule display the strongest orientation correlations. This can be explained by the close-packed nature of this arrangement and the favourable interaction of the hydrogen atoms with the charge density in the cavity between the three bromine atoms. The lower OCF intensity at position (1) at θ=0° compared to position (1) at 180° indicates that molecules directly above the reference molecule do not display as strong orientation correlations as the molecules underneath.

A weak preference for anti-collinear alignment of the dipole moments of molecules with close bromine atoms can be observed (structure 2), which may be due to halogen bonding.[30,31] A slightly larger preference for anti-collinear alignment with close hydrogen atoms is observed (structure 3), which is consistent with the close H–H contacts seen in Figure 2.

On the basis of this analysis, it can be concluded that bromoform also displays preferential stacking with collinear alignment of the dipole moments as observed for chloroform.[8] However, the orientation correlations are overall less pronounced and there are larger numbers of anti-collinear arrangements with close hydrogen atoms.

Comparison of Kirkwood correlation factors from the EPSR model and dielectric spectroscopy

To test the EPSR model of bromoform, it is instructive to compare the Kirkwood correlation factors estimated from the structural model with those from dielectric

spectroscopy. In general, the Kirkwood correlation factor, g_K, is a measure of the net relative dipole alignments of polar molecules in liquids[32,33] and is defined as

$$g_K = 1 + N\langle \cos \alpha \rangle \quad (1)$$

where N is the number of contributing molecular dipoles and <cos α> the average of the cosines of the relative dipole alignments. A liquid with a g_K of one contains no preferred dipole alignments. Parallel or antiparallel dipole alignments are indicated by g_K values greater or smaller than one, respectively.

Using the Kirkwood-Fröhlich equation, g_K can be estimated from the static dielectric constant ε of a liquid, its high-frequency dielectric constant ε_∞, the vapour-phase dipole moment of the polar molecule μ_0 and the number density of molecules ρ.[32,34,35]

$$g_K = \frac{(\varepsilon-\varepsilon_\infty)(2\varepsilon+\varepsilon_\infty)}{\varepsilon(\varepsilon_\infty+2)^2} \cdot \frac{9\varepsilon_0 kT}{\rho\mu_0^2} \quad (2)$$

In ref. [8], we estimated the g_K of chloroform from literature data as 1.26 at 25°C, but values of 1.40 and 1.30 can also be found in the literature.[36,37] For bromoform, g_K has been reported as 0.80[37] suggesting a preference for antiparallel alignment of dipole moments in contrast to chloroform. Using the quantities listed in refs [22,38], we estimate a value of 0.86 for bromoform at 293 K using the Kirkwood-Fröhlich equation.

The g_K factor can also be estimated from an *EPSR*-derived structural model using the $h_{\text{COM-COM}}(l=1, l_1=1, l_2=0; n_1=0, n_2=0; r)$ correlation function, which contains the information on relative dipole alignments and is obtained from spherical-harmonic expansion.[39] In the limit of $r_{\max} \rightarrow \infty$, $g_K(r_{\max})$ equals g_K.

$$g_K(r_{\max}) = 1 - \frac{1}{3\sqrt{3}}\rho \int_0^{r_{\max}} 4\pi r^2 \, h_{\text{COM-COM}}(110; 00; r)\, dr \quad (3)$$

Figure 5 shows the distance-dependant $g_K(r_{max})$ function obtained from the EPSR model of liquid bromoform together with the corresponding function of liquid chloroform from ref. [8]. Consistent with the g_K values from dielectric spectroscopy, $g_K(r_{max})$ of bromoform is always smaller than that of chloroform. The initial rise in $g_K(r_{max})$ at around r_{max} = 5 Å reflects the presence of polar stacks of molecules in bromoform. After this, the function seems to decrease above 13 Å. However, this is accompanied by considerable increases of the associated margins of error. Considering that we have higher confidence in the initial rise in $g_K(r_{max})$ and that dielectric spectroscopy suggests $g_K < 1$, requires $g_K(r_{max})$ to decrease eventually after the initial rise. This suggests that the longer-range structure of bromoform is ultimately responsible in giving a g_K value lower than one and hence net antiparallel dipole alignments.

It is important to keep in mind the sources and magnitudes of error associated with both avenues for obtaining g_K. The limitations in obtaining accurate g_K values from structural models are that the box size limits integration to finite values of r_{max}, and the increasing contributions of noise at larger distances, which are amplified by the r^2 term in equation 3. The g_K values derived from dielectric spectroscopy can also be affected by systematic errors due to simplifications made in the derivation of the Kirkwood-Fröhlich equation.[34,40] These include a spherical shape of the molecule in question and the requirement that the molecule is embedded within a matrix with a dielectric constant of ε_∞. Furthermore, ε_∞ is often difficult to measure experimentally and g_K can respond in a very sensitive manner to small changes in the various quantities. For example, if ε_∞ is calculated using the Maxwell relation ($\varepsilon_\infty=n^2$) where n is the refractive index,[41] a value of 1.00 is obtained for the g_K of bromoform. However, it needs to be stressed that this was the by far the largest value obtained for g_K using a wide range of different quantities from the literature for the Kirkwood-Fröhlich equation. Overall, it is fair to state that

dielectric spectroscopy measurements suggest a preference for at least weak antiparallel alignment of dipole moments in bromoform.

Conclusions

EPSR models are now available for both liquid haloforms. Despite some structural similarities, such as the existence of polar stacks of molecules, bromoform displays weaker orientation correlations and more spatially defined close intermolecular contacts than chloroform. The net tendency for antiparallel dipole alignment in bromoform, as suggested by the Kirkwood correlation factor from dielectric spectroscopy, is most likely caused by weak but persistent long-range orientation correlations.

Since the molecular dipole moments of bromoform and chloroform are quite similar,[6] the observed structural differences between the two liquids are unlikely to arise from different dipolar interactions. We speculate that halogen bonding, which is expected to be stronger for bromoform,[31,42] is responsible for a stronger tendency for antiparallel arrangements including the configurations with close contacts of the fully brominated faces and with close H-H contacts. In this context, it is interesting to note that the improvements to the fits of the neutron diffraction data upon switching on the empirical potentials were accompanied by complex changes in $g_{\mathrm{Br\text{-}Br}}(r)$, which implies that the halogen bonding was not reproduced well by the starting potentials. Ultimately, these points will need to be clarified with high-level molecular dynamics simulations capable of including the multipolar interactions required for describing halogen bonding.

Finally, in this work we have highlighted the usefulness of benchmarking the Kirkwood correlation factor from the diffraction-derived structural model against the one from dielectric spectroscopy. In future studies, it could make sense to use the g_{K} value from dielectric spectroscopy as a constraint for running EPSR simulations with large box sizes. It would then be possible to obtain structural models for which the local and

intermediate-range structure is consistent with the diffraction data, and the long-range structure in agreement with dielectric spectroscopy. Such an approach could benefit the structural analysis of a wide range of molecular liquids and solvents including ionic liquids[43].

Acknowledgments

We thank the Royal Society for a University Research Fellowship (CGS), the EPSRC and Durham University for a PhD studentship (JJS), the ISIS neutron source for granting access to the SANDALS beamline, S. Imberti and S. Callear for help during the neutron diffraction experiment, and A. Soper for helpful discussions.

Declaration of interest statement

No interest to declare.

References

[1] S. Pothoczki, L. Temleitner, and L. Pusztai, *Chem. Rev.* **115** (24), 13308 (2015).

[2] R. C. Fuson and B. A. Bull, *Chem. Rev.* **15** (3), 275 (1934).

[3] S. Kyasa, *Synlett.* **26** (13), 1911 (2015).

[4] A. Puckner, *J. Am. Chem. Soc.* **23**, 470 (1901).

[5] M. J. Solomon and F. A. Crane, *J. Pharm. Sci.* **59**, 1680 (1970).

[6] F. Bertolotti and G. Gervasio, *J. Mol. Struct.* **1036**, 305 (2013).

[7] R. Myers, B. H. Torrie, and B. M. Powell, *J. Chem. Phys.* **79** (3), 1495 (1983); T. Kawaguchi, K. Takashina, T. Tanaka, and T. Watanabe, *Acta Cryst. B* **28** (3), 967 (1972); K. F. Dziubek and A. Katrusiak, *J. Phys. Chem. B* **112** (38), 12001 (2008).

[8] J. J. Shephard, A. K. Soper, S. K. Callear, S. Imberti, J. S. O. Evans, and C. G. Salzmann, *Chem. Comm.* **51** (4770-4773) (2015).

[9] A. K. Soper, *Chem. Phys.* **202**, 295 (1996); A. K. Soper, *Phys. Rev. B* **72**, 104204 (2005).

[10] C. Andreani, M. A. Ricci, M. Nardone, M. A. Ricci, and A. K. Soper, *J. Chem. Phys.* **107**, 214 (1997); C. Andreani, *J. Mol. Liq.* **78**, 217 (1998).

[11] S. E. McLain, C. J. Benmore, J. E. Siewenie, J. Urquidi, and J. F. C. Turner, *J. Am. Chem. Soc.* **43**, 1952 (2004); A. K. Soper, *J. Chem. Phys.* **101**, 6888 (1994); G. Santoli, F. Bruni, M. A. Ricci, and A. K. Soper, *Mol. Phys.* **97**, 777 (1999); J. Neuefeind, H. E. Fischer, and W. Schröer, *J. Phys.: Condens. Matter* **12**, 8765 (2000); N. S. Basma, T. F. Headen, M. S. P. Shaffer, N. T. Skipper, and C. A. Howard, *J. Phys. Chem. B* **122** (38), 8963 (2018).

[12] C. Andreani, F. Menzinger, M. A. Ricci, A. K. Soper, and J. Dreyer, *Phys. Rev. B* **49**, 3811 (1994); A. K. Soper, C. Andreani, and M. Nardone, *Phys. Rev. E* **47**, 2598 (1993).

[13] H. Bertagnolli and P. Chieux, *Mol. Phys.* **51** (3), 617 (1984).

[14] S. Pothoczki, L. Temleitner, S. Kohara, P. Jovari, and L. Pusztai, *J. Phys. Condens. Matter* **22**, 404211 (2010).

[15] L. Pusztai, *Mol. Simul.* **1** (6), 359 (1988).

[16] H. Bertagnolli, K. Goller, and H. Zweier, *Ber. Bunsenges. Phys. Chem.* **99**, 1168 (1995).

[17] S. Pothoczki, L. Temleitner, and L. Pusztai, *J. Chem. Phys.* **134**, 044521 (2011).

[18] J. J. Karnes and I. Benjamin, *J. Mol. Liq.* **248**, 121 (2017).

[19] J. J. Shephard, S. K. Callear, S. Imberti, J. S. O. Evans, and C. G. Salzmann, *Phys. Chem. Chem. Phys.* **18** (28), 19227 (2016).

[20] R. Rey, *J. Chem. Phys.* **126** (2007).

[21] A. K. Soper, *Molecular Physics* **107**, 1667 (2009).

[22] B. Horváth and I. Szalai, *J. Mol. Liq.* **189**, 81 (2014).

[23] Q. Williams, J. T. Cox, and W. Gordy, *J. Chem. Phys.* **20** (10), 1524 (1952).

[24] A. Habartová, K. T. Valsaraj, and M. Roeselová, *J. Phys. Chem. A* **117** (38), 9205 (2013).

[25] C. G. Gray and K. E. Gubbins, *Theory of Molecular Fluids, Volume 1: Fundamentals* (Clarendon Press, Oxford, 1984).

[26] A. K. Soper, in *Local Structure from Diffraction*, edited by S. J. Billinge and M. F. Thorpe (Plenum Press, New York, 1998).

[27] J. M. Zaug, A. K. Soper, and S. M. Clark, *Nat. Mat.* **7**, 890 (2008).

[28] I. M. Svishchev and P. G. Kusalik, *J. Chem. Phys.* **99**, 3049 (1993).

[29] A. K. Soper, *J. Chem. Phys.* **101** (8), 6889 (1994).

[30] F. F. Awwadi, R. D. Willett, K. A. Peterson, and B. Twamley, *Chem. Eur. J.* **12** (35), 8952 (2006); M. R. Scholfield, C. M. V. Zanden, M. Carter, and P. S. Ho, *Protein Sci.* **22** (2), 139 (2013).

[31] P. Politzer, J. S. Murray, and T. Clark, *Phys. Chem. Chem. Phys.* **15**, 11178 (2013).

[32] J. G. Kirkwood, *J. Chem. Phys.* **7**, 911 (1939).

[33] N. Deba, A. S. Tiwaryb, and A. K. Mukherjee, *Mol. Phys.* **108**, 1907 (2010).

[34] H. Fröhlich, *Trans. Faraday Soc.* **44**, 238 (1948); J. C. R. Reis and T. P. Iglesias, *Phys. Chem. Chem. Phys.* **13** (22), 10670 (2011).

[35] P. H. Fries, *Mol. Phys.* **90**, 841 (1997); L. Onsager, *J. Am. Chem. Soc.* **58** (8), 1486 (1936).

[36] T. Sigvartsen, B. Gestblom, E. Noreland, and J. Songstad, *Acta Chem. Scand.* **43**, 103 (1989).

[37] Y. Marcus, *J. Solution Chem.* **21** (12), 1217 (1992).

[38] *Broadband Dielectric Spectroscopy* (Springer-Verlag Berlin Heidelberg, 2003).

[39] A. K. Soper, *J. Chem. Phys.* **101** (8), 6888 (1994).

[40] M. Valiskó and D. Boda, *J. Phys. Chem. B* **109** (13), 6355 (2005).

[41] L. Simeral and R. L. Amey, *J. Phys. Chem.* **74**, 1443 (1970).

[42] D. S. Yufit, R. Zubatyuk, O. V. Shishkin, and J. A. K. Howard, *CrystEngComm* **14** (23), 8222 (2012); W. L. Jorgensen and P. Schyman, *J. Chem. Theory Comput.* **8** (10), 3895 (2012).

[43] C. Hardacre, J. D. Holbrey, M. Nieuwenhuyzen, and T. G. A. Youngs, *Acc. Chem. Res.* **40** (11), 1146 (2007); R. Hayes, G. G. Warr, and R. Atkin, *Chem. Rev.* **115** (13), 6357 (2015).

Tables

Table 1. Average bond lengths, $r_{A–B}$, and angles, $\gamma_{A–B–C}$,[23] Lennard-Jones parameters, σ and ε, and partial charges, q,[24] used for the starting configuration of the EPSR simulation.

$r_{C–Br}$ / Å	1.930		
$r_{C–H}$ / Å	1.092		
$\gamma_{Br–C–Br}$ / °	110.48		
$\gamma_{H–C–Br}$ / °	108.47		
σ / Å	C: 3.40	H: 2.50	Br: 4.00
ε / kJ mol^{-1}	C: 0.46	H: 0.07	Br: 1.34
q / e	C: –0.77	H: 0.41	Br: 0.12

Figures

Figure 1

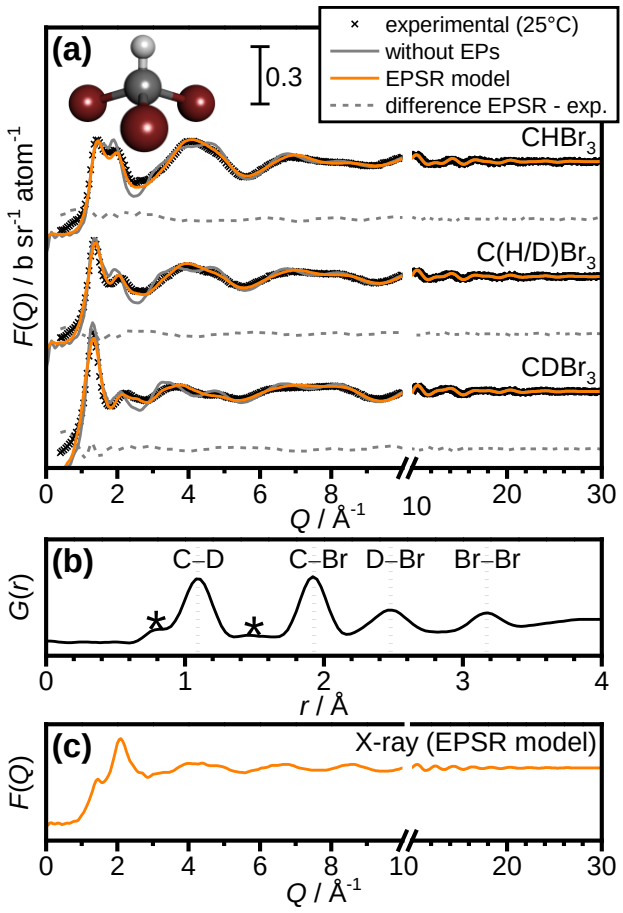

Figure 2

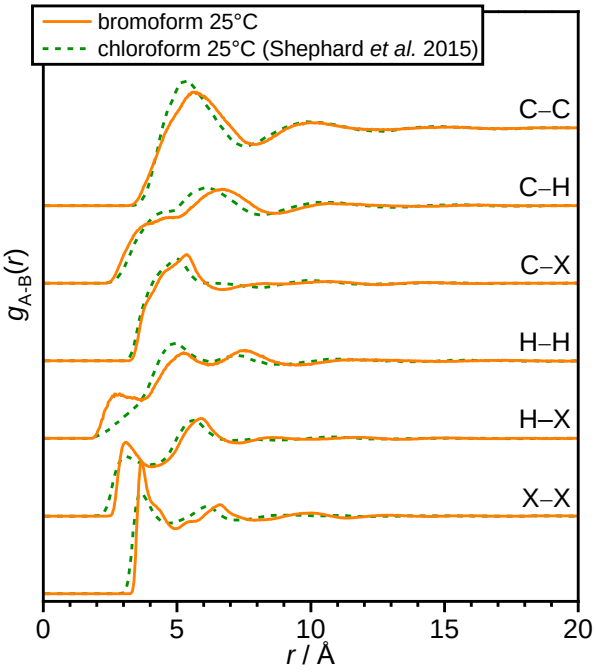
bromoform 25°C
chloroform 25°C (Shephard et al. 2015)
C–C
C–H
C–X
H–H
H–X
X–X
$g_{A\text{-}B}(r)$
0
5
10
15
20
r / Å

Figure 3

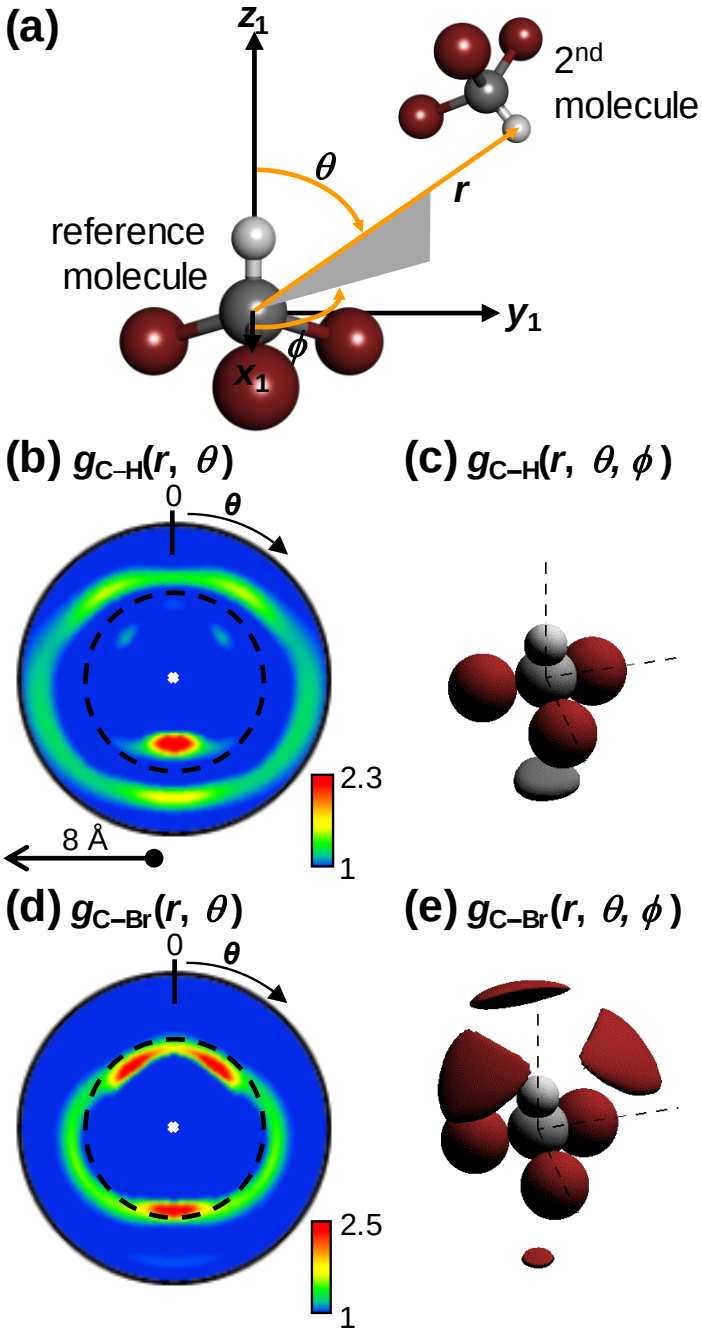
(a)
z_1
2nd molecule
θ
r
reference molecule
y_1
ϕ
x_1
(b) $g_{C-H}(r, \theta)$
0
θ
2.3
1
8 Å
(c) $g_{C-H}(r, \theta, \phi)$
(d) $g_{C-Br}(r, \theta)$
0
θ
2.5
1
(e) $g_{C-Br}(r, \theta, \phi)$

Figure 4

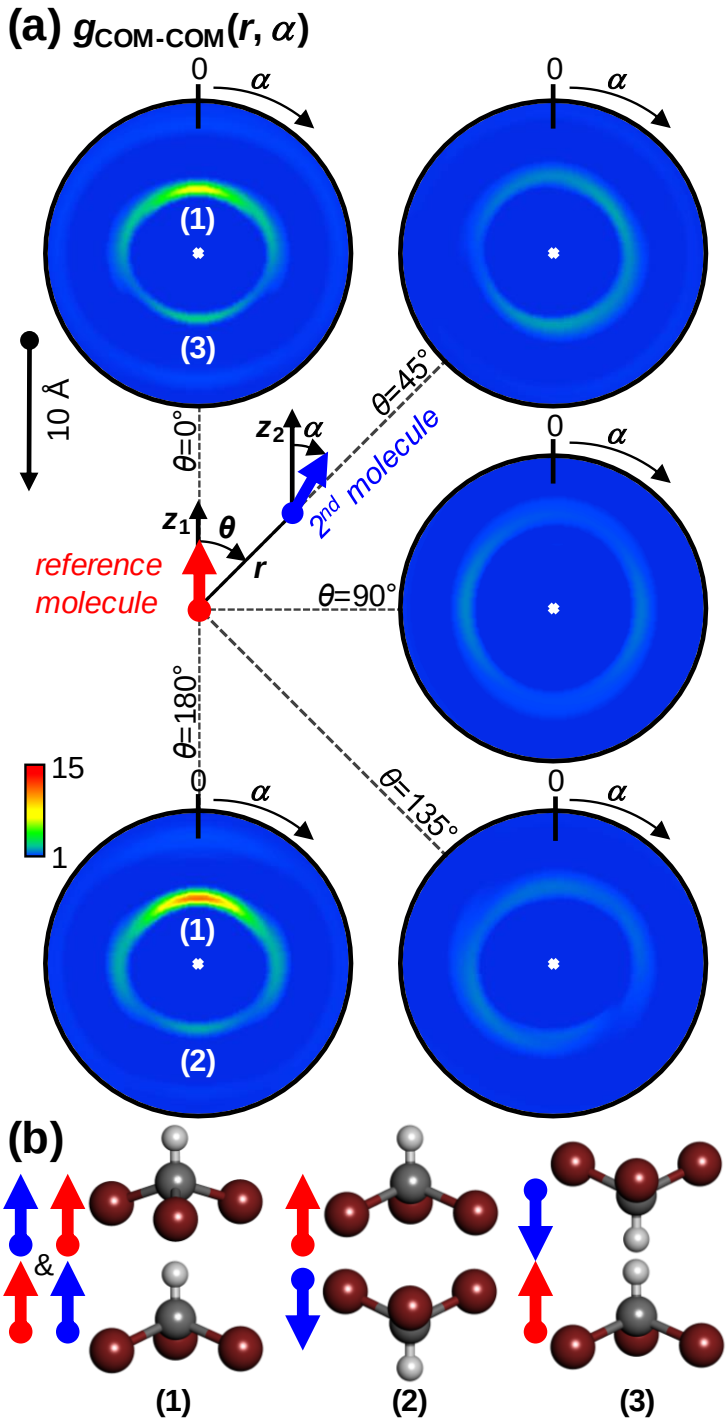
(a) $g_{COM\text{-}COM}(r, \alpha)$
0
α
(1)
(3)
(2)
10 Å
θ=0°
θ=45°
θ=90°
θ=135°
θ=180°
z_1
z_2
θ
r
reference molecule
2nd molecule
15
1
(b)
&
(1)
(2)
(3)

Figure 5

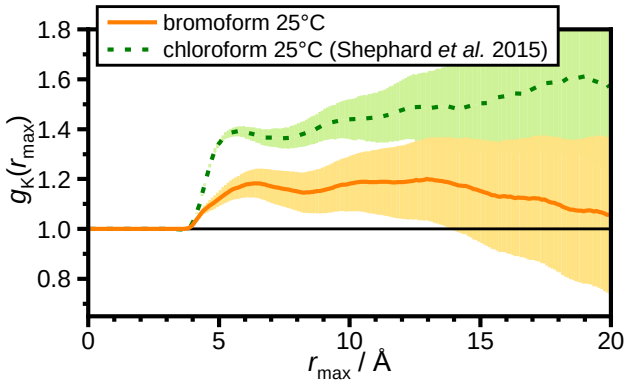
bromoform 25°C
chloroform 25°C (Shephard *et al.* 2015)
1.8
1.6
1.4
1.2
1.0
0.8
$g_K(r_{max})$
0
5
10
15
20
r_{max} / Å

Figure captions

Figure 1. (a) Experimental (black crosses) and calculated neutron total structure factors of liquid bromoform at 25°C including $CHBr_3$, $C(H/D=50/50)Br_3$ and $CDBr_3$ samples. The calculated data is shown for EPSR simulations not using empirical potentials (solid grey lines) and after including empirical potentials (solid orange lines). The differences between the experimental data and the EPSR fits are shown as dashed grey lines which have been shifted downwards for clarity. The molecular structure of bromoform is shown in the inset with brown, grey and white spheres representing bromine, carbon and hydrogen atoms, respectively. (b) Intramolecular part of the $G(r)$ pair distribution function obtained from the experimental $F(Q)$ of $CDBr_3$. The various intramolecular atomic distances defined in the input to EPSR are highlighted by dashed orange vertical lines. Features indicated by asterisks are Fourier-transform artefacts. (c) Calculated X-ray structure factor of the neutron-derived EPSR model.

Figure 2. Intermolecular $g_{A\text{-}B}(r)$ pair-correlation functions of liquid bromoform (solid orange lines) and chloroform (dashed green lines) at 25°C. The chloroform data was taken from ref. [8].

Figure 3. (a) Illustration showing the spherical coordinates that define the positions of atoms of a 2nd molecule in the coordination of a reference molecule in a fixed orientation. (b, d) Contour plots of $g_{C–H}(r, \theta)$ and $g_{C–Br}(r, \theta)$, respectively. The dashed circles indicate radial distances of 4.7 Å, which were used as the upper limits for creating the spatial density functions in (c) $g_{C–H}(r, \phi, \theta)$ and (e) $g_{C–Br}(r, \phi, \theta)$ both plotted with fractional isosurface levels of 0.1.

Figure 4. (a) Contour plots of the centre-of-mass to centre-of-mass pair-correlation functions $g_{COM–COM}(r, \alpha)$ for specified values of θ. The relative orientation of the dipole moment of a 2nd molecule is defined by the angle α and r is the centre of mass separation. The structures corresponding to positions (1-3) are shown in (b).

Figure 5. The distance-dependent Kirkwood correlation function $g_K(r_{max})$ derived from the EPSR structural model of liquid bromoform. The corresponding data for liquid chloroform was taken from ref. [8]. The shaded areas indicate the estimated error.